Experimental observation of periodic Korteweg-de Vries solitons along a torus of fluid

Filip Novkoski, Chi-Tuong Pham, Eric Falcon

Experimental observation of periodic Korteweg-de Vries solitons along a torus of fluid

Filip Novkoski[1] [(a)], Chi-Tuong Pham[2] [(b)] and Eric Falcon[1] [(c)]

[1] *Université Paris Cité, CNRS, MSC, UMR 7057, F-75013 Paris, France*
[2] *Université Paris-Saclay, CNRS, LISN, UMR 9015, F-91405 Orsay, France*

Abstract –We report on the experimental observation of solitons propagating along a torus of fluid. We show that such a periodic system leads to significant differences compared to the classical plane geometry. In particular, we highlight the observation of subsonic elevation solitons, and a nonlinear dependence of the soliton velocity on its amplitude. The soliton profile, velocity, collision, and dissipation are characterized using high resolution space-time measurements. By imposing *periodic boundary conditions* onto Korteweg-de Vries (KdV) equation, we recover these observations. A nonlinear spectral analysis of solitons (periodic inverse scattering transform) is also implemented and experimentally validated in this periodic geometry. Our work thus reveals the importance of periodicity for studying solitons and could be applied to other fields involving periodic systems governed by a KdV equation.

Introduction. – Since their first observation on the surface of water [1], solitons have been widely studied in various domains (including acoustics [2], plasmas [3], carbon nanotubes [4], Bose–Einstein condensates [5, 6], or blood vessels of living organisms [7]). Korteweg and de Vries (KdV) first provided an analytical description of solitons [8], which can be observed as either waves of elevation [9] or depression [10] on the surface of a fluid. Although KdV solitons have mainly been investigated experimentally in rectilinear geometries [9–13], examples in both curved and periodic media remain elusive.

A stable torus of fluid is a good experimental system to study solitons in a curved and periodic geometry. We manage to create such a stable torus of liquid by means of an original technique. We have previously studied linear waves propagating along the inner and outer torus borders [14]. Here, using this technique, we experimentally discover unreported periodic KdV solitons along a stable torus of liquid whose properties are fully characterized (profile, velocity, collision, and dissipation), and described with an experimentally validated model taking into account both the curved and periodic conditions. Our work thus paves the way to observe other nonlinear phenomena such as wave turbulence [15, 16], and soliton gas [17–21] in this specific geometry. Note that KdV solitons can be reached experimentally in curved geometries without periodicity (*e.g.,* along the border of a liquid cylinder [22–24]), whereas trials have been attempted for periodic conditions in plane geometry (*e.g.,* in an annular water tank [25,26]), as well as for a curved and periodic system but only in a nonstationary regime and by applying a strong constraint to the liquid ring [27–29].

Theoretical works on solitons have yielded advanced mathematical techniques to study solutions to various integrable nonlinear equations [*e.g.,* KdV, Nonlinear Schrödinger (NLS), Kadomtsev-Petviashvili], in particular the inverse scattering transform (IST) [30–33]. This nonlinear spectral analysis has been applied to experimental NLS solitons [21, 33], but remain scarce for KdV ones [34–36], and, so far, have not been applied to a periodic experimental system, a more complex setting which has recently received numerical and theoretical attention [33, 37–39].

Experimental setup. – We manage to create a stable torus of fluid by depositing distilled water on a superhydrophobic duralumin plate machined with a slightly sloping triangular groove along the perimeter (see fig. 1a-c) [14]. The radius of the groove center, R, is either 4 cm or 7 cm using two different substrates. The small angle α of the groove to the horizontal is 4.5°. We use a commercial superhydrophobic coating yielding a contact angle of 160°–170° between liquid and substrate [14, 40]

[(a)] filip.novkoski@u-paris.fr
[(b)] chi-tuong.pham@upsaclay.fr
[(c)] eric.falcon@u-paris.fr (corresponding author)

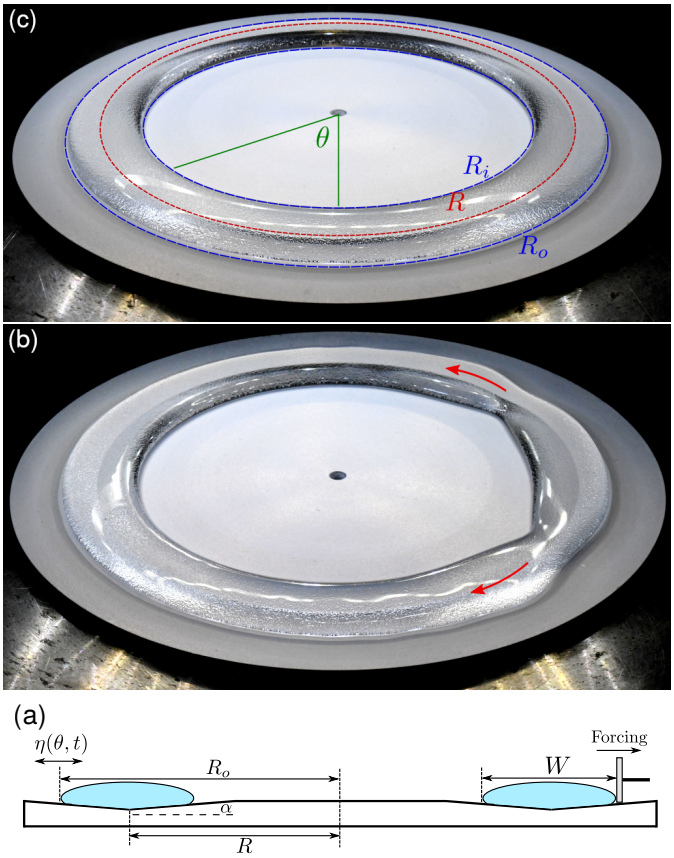

Fig. 1: a) Schematic profile of the experimental setup. b) Solitons propagating along the torus borders. c) Stable liquid torus on a plate ($R_o = 7.9\,\mathrm{cm}$, $R = 7\,\mathrm{cm}$, $W = 1.8\,\mathrm{cm}$).

allowing the liquid torus to move with almost no constraint. To generate waves, the torus is impulse pulled (or pushed) horizontally using a linear actuator with a teflon plate attached to its end (see fig. 1a). By deforming the meniscus, the actuator creates two counter-propagating solitons along the outer, and two along the inner, border of the torus (see fig. 1b and movies in Supp. Mat. [41]). A camera located above the torus records the displacements of the two interfaces. Using a border detection algorithm [42], we extract the azimuthal displacement $\eta(\theta, t)$, in the horizontal plane, of both the inner and outer torus borders. Measurements are made for various pulse amplitudes and for different torus widths, W, by adding water. We set $\chi = R_o/R$ in order to quantify the system curvature, with R_o the outer radius of the torus, and $R_o = R + W/2$ with W the torus width (see fig. 1a). KdV solitons in the toroidal geometry will be characterized using the $R = 7$ cm case. The effects of periodicity on the solitons will be evidenced by decreasing the radius to $R = 4$ cm.

Soliton solutions. – When weak dispersion is balanced by weak nonlinearity in a shallow water regime, azimuthal waves $\eta(\theta, t)$ along a torus of fluid are governed at the leading order by an ad hoc KdV equation with *periodic boundary conditions* as

$$\eta_t + \Omega_0 \left[\eta_\theta + \frac{5\chi^2}{4\widetilde{W}} \eta\eta_\theta + \frac{\chi^2 \widetilde{W}^2}{2R^2} \delta_{\mathrm{Bo}} \eta_{\theta\theta\theta} \right] = 0\,, \qquad (1)$$

with $\widetilde{W} = W/2$, $\delta_{\mathrm{Bo}} = \mathrm{Bo}_c - \mathrm{Bo}$, and $\Omega_0 = (g_{\mathrm{eff}}\widetilde{W})^{1/2}/R$ the angular phase velocity of linear gravity waves. The Bond number reads $\mathrm{Bo} = \ell_{\mathrm{eff}}^2/(\widetilde{W}^2\chi^4)$, $\mathrm{Bo}_c \approx 1/6$, where $\ell_{\mathrm{eff}} \equiv \sqrt{\sigma_{\mathrm{eff}}/(\rho g_{\mathrm{eff}})}$ is the effective capillary length, $\rho = 10^3\,\mathrm{kg\,m^{-3}}$ is the fluid density, $g_{\mathrm{eff}} = g\sin\alpha$ is the effective gravity, and $g = 9.81\,\mathrm{m\,s^{-2}}$. $\sigma_{\mathrm{eff}} \simeq 60\,\mathrm{mN\,m^{-1}}$ is an effective surface tension inferred from the low-amplitude (linear regime) measurement of the dispersion relation. g_{eff} and σ_{eff} are strongly linked to the substrate geometry and renormalization effects [24]. We obtain eq. (1) using a Taylor expansion of the gravity-capillary dispersion relation along a liquid torus [14], and adapting nonlinear corrections introduced in [24] for a rectilinear fluid cylinder to our torus geometry (see Supp. Mat [41]).

Cnoidal wave solutions to eq. (1) read

$$\eta(\theta, t) = A\,\mathrm{cn}^2\left(\frac{\theta - \Omega t}{\Delta\sqrt{m}}\middle| m\right) \text{ with } \Delta^2 = \frac{24}{5}\frac{\widetilde{W}^3}{AR^2}\delta_{\mathrm{Bo}}, \quad (2)$$

where A is the (signed) amplitude and Δ the (angular) width of the solitary wave. The sign of A is given by that of δ_{Bo}. The velocity of the soliton of eq. (2) reads

$$\Omega = \Omega_0\left[1 + \frac{5A}{6\widetilde{W}m}\chi^2\left(1 - \frac{m}{2} - \frac{3\,\mathrm{E}(m)}{2\,\mathrm{K}(m)}\right)\right]. \qquad (3)$$

$\mathrm{K}(m)$ [resp. $\mathrm{E}(m)$] is the complete elliptic integral of the first (resp. second) kind. $m \in [0, 1]$ is the elliptic parameter for which the cnoidal function $\mathrm{cn}(\theta|m)$ is $\cos(\theta)$ for $m = 0$, and $\mathrm{sech}(\theta)$ for $m = 1$ [13, 44]. Although the cnoidal wave is a periodic function, the 2π-periodicity condition on the circle (*i.e.,* torus border) still has to be ensured, and reads

$$\frac{2\pi}{N_\theta\Delta} = 4K(m),\ \textit{i.e.},\quad \pi = 2N_\theta\sqrt{\frac{6\tilde{W}^3 m\delta_{\mathrm{Bo}}}{5R^2A}}\,\mathrm{K}(m)\,, \quad (4)$$

with N_θ the number of solitons. The parameter m and the amplitude A have thus a nontrivial relationship (see below). The periodic elliptic solutions of eq. (2) are close to sech^2 for large enough R (*e.g.,* for $R = 7\,\mathrm{cm}$, $1 - m \simeq 10^{-12}$). In that case, eqs. (2) and (3) reduce to the classical solitary wave profile $\eta(\theta, t) = A\,\mathrm{sech}^2[(\theta - \Omega t)/\Delta]$ and velocity $\Omega = \Omega_0[1 + 5A\chi^2/(12\widetilde{W})]$. However, for smaller R (e.g. 4 cm), this classical solution cannot be used since the effect of periodicity, through eq. (4), has to be taken into account (see below). Note that the experimental parameters used here are in the range of validity required for the derivation of eq. (1) assuming weak dispersion $\mu = \widetilde{W}^2\chi^2\delta_{\mathrm{Bo}}/(\Delta^2R^2) \in [0.05, 0.3] \ll 1$ (*i.e.,* shallow-water limit), weak nonlinearity $\epsilon = A\chi^2/\widetilde{W} \in [0.005, 0.2] \ll 1$, both of the same order of magnitude $\mu/\epsilon = \widetilde{W}^3/(\Delta^2R^2A) \in [1, 3]$.

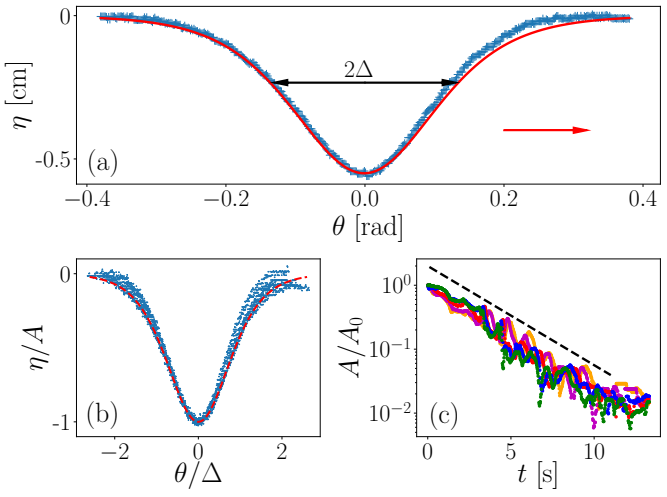

Fig. 2: a) (+) Experimental soliton profile at a fixed time. (−) Theoretical profile of eq. (2) with no fitting parameter. b) Superimposition of rescaled soliton profiles during its propagation along one torus perimeter. (−) eq. (2). c) Exponential damping of the soliton for different $W \in [2.2, 3]$ cm (2 mm step). $R = 7$ cm. Dashed line of slope $\tau = 2.8$ s.

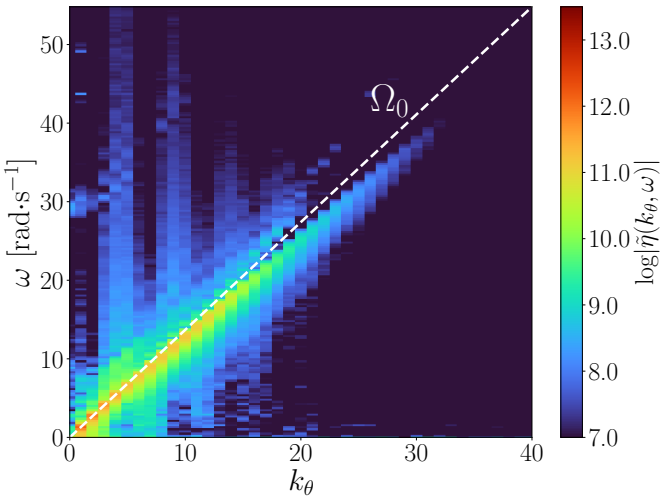

Fig. 3: Space-time Fourier spectrum $\tilde{\eta}(k_\theta, \omega)$ of the signal $\eta(\theta, t)$ (outer border). Dashed line: velocity $\Omega_0 = 1.37$ rad/s of long linear waves. The energy is concentrated around a linear branch of slope $\Omega < \Omega_0$, signature of a subsonic soliton.

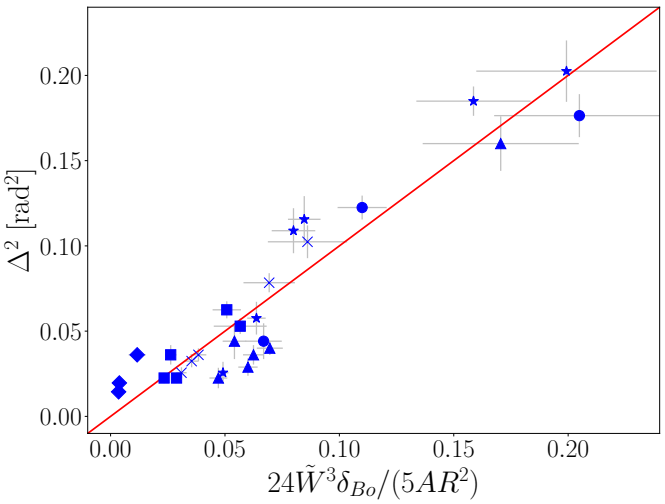

Fig. 4: Experimental soliton width squared Δ^2 for different amplitudes A and different widths $W \in [1.9, 4]$ cm (2 mm step). $R = 7$ cm. Solid line: eq. (2) with no fitting parameter (slope 1).

Soliton profile. – The pulse profile, $\eta(\theta, t)$, is extracted from the outer torus border (*e.g.,* from the depression in fig. 1b). Figure 2a shows that the experimental profile is well described by the theoretical soliton profile of eq. (2) with no fitting parameter. Since a soliton balances theoretically dispersion and nonlinearity, it should also have a self-similar profile during its propagation. Figure 2b shows the superimposed rescaled profiles of a soliton during its propagation along almost one torus perimeter. The soliton (with this appropriate rescaling) thus conserves a self-similar shape during its propagation that is well described by eq. (2), even if its amplitude decreases due to unavoidable dissipation. To quantify the latter, we plot in fig. 2c the soliton amplitude as a function of time, $A(t)$, during two rounds along the torus. $A(t)/A(0)$ is found to decrease exponentially as $A(t) = A(0)\exp[-t/\tau]$, with a damping time τ found to be independent of the viscosity of the fluid used ($\nu \in [10^{-7}, 10^{-6}]\,\mathrm{m}^2/\mathrm{s}$, *i.e.,* mercury or water). This suggests that dissipation does not come from viscous dissipation, but probably from the pinning of the triple contact line [43]. Indeed, the capillary number $\mathrm{Ca} = \rho\nu\Omega\mathrm{R}/\sigma_{\mathrm{eff}} \in [10^{-6}, 10^{-3}]$ leads to dominant interfacial forces with respect to viscous ones.

Fourier spectrum. – We now compute the space-and-time Fourier transform, $\tilde{\eta}(k_\theta, \omega)$, of the signal $\eta(\theta, t)$ as shown in fig. 3. The energy is found to be concentrated around a line of slope $\Omega = \omega/k_\theta$ corresponding to the pulse velocity. This quasi-nondispersive feature is a spectral signature of a soliton. The soliton velocity, Ω, is found to be slightly slower than long linear waves propagating at velocity Ω_0 (see fig. 3), meaning the presence of a subsonic soliton. Note that a broadening of the soliton branch occurs due to nonlinearities, whereas low-intensity vertical traces (at low k_θ) correspond to mechanical noise.

Soliton width and velocity. – We now measure the typical soliton width Δ by fitting eq. (2) to the experimental profile (as in fig. 2a). Δ^2 is plotted in fig. 4 for different pulse amplitudes, A, and torus widths W. Δ is found to scale as $\sqrt{W^3/A}$ in good agreement with eq. (2)b with no fitting parameter (see solid line), thus justifying our ad hoc model that will lead to further predictions (see below). We also measure the soliton velocity by time of flight during its propagation. The dimensionless pulse velocity, Ω/Ω_o (*i.e.,* Froude number), is displayed in fig. 5 for various A

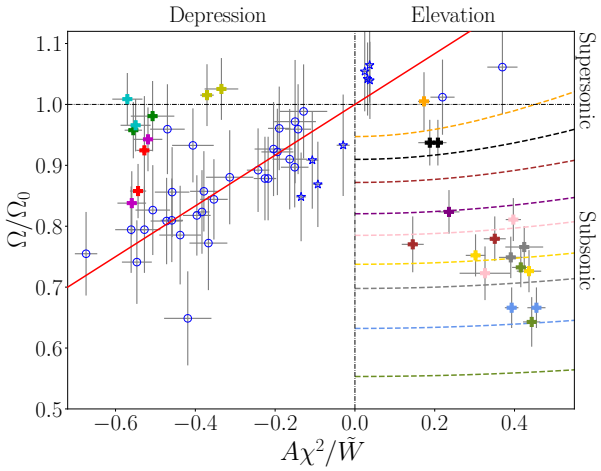

Fig. 5: Dimensionless soliton velocity Ω/Ω_o versus $A\chi^2/W$ for various A and W for $R = (+)$ 4 and $(\circ)$ 7 cm. Dashed lines: eq. (3) for different $W \in [2.8, 3.9]$. Solid line: classical KdV solution (slope 5/12). Occurrence of subsonic elevation solitons is due to effects of the periodic geometry.

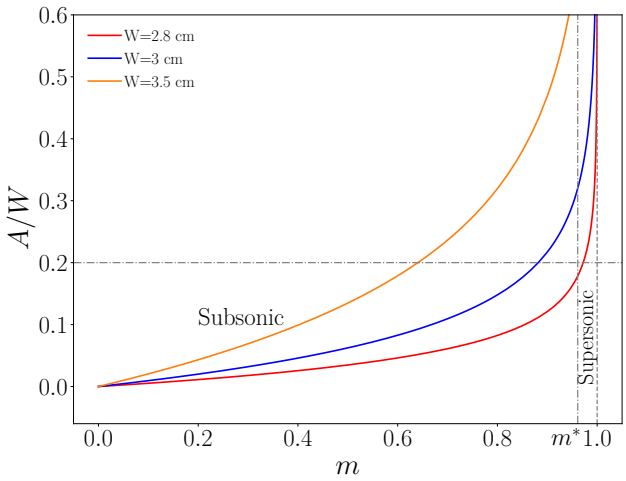

Fig. 6: Theoretical dependence of the elevation soliton amplitude A on the parameter m for different torus widths W, using eq. (4) with $N_\theta = 2$ and $R = 4$ cm. $m^* = 0.96$ corresponds to the transition between subsonic and supersonic elevation solitons. The horizontal line ($A/W = 0.2$) corresponds to the maximal soliton amplitude reachable experimentally. This thus limits attainable values of m, thus restricting the observation to the subsonic case for elevation solitons ($\delta_{\mathrm{Bo}} > 0$, *i.e.*, $\mathrm{Bo} < \mathrm{Bo}_c$).

and W. For large tori (*i.e.*, using the substrate $R = 7$ cm for various W), the soliton velocity of eq. (3) reduces to the classical KdV linear relationship, $\Omega/\Omega_0 = 1+5A\chi^2/(12\widetilde{W})$ (see solid line), which is well verified experimentally (open circles). Depression solitons ($A < 0$) moving slower than linear waves ($\Omega/\Omega_0 < 1$ or subsonic) are observed for $\mathrm{Bo} > \mathrm{Bo}_c$, whereas elevation solitons ($A > 0$) are supersonic ($\Omega/\Omega_0 > 1$) for $0 \leq \mathrm{Bo} < \mathrm{Bo}_c$, as predicted for KdV in straight geometry [8, 10]. For smaller tori (*i.e.*, $R = 4$ cm substrate), the relationship of eq. (3) between velocity and amplitude is no longer linear (see dashed lines from eq. (3) for different W). In particular, we clearly observe *subsonic elevation* solitons due to the effects of the periodic geometry (see + in the bottom right quadrant).

Periodicity effects on the soliton velocity. – The transition from subsonic to supersonic solitons occurs, from eq. (3), at $m^* = 2 - 3E(m^*)/K(m^*) \simeq 0.96$ regardless of Bo. This leads to different solutions of the periodic KdV equation as follows

δ_{Bo}	Type	$0 < m < m^*$	$m^* < m < 1$
> 0	Elevation	Subsonic	Supersonic
< 0	Depression	Supersonic	Subsonic

An additional effect of the periodicity condition eq. (4) is that certain types of solitons are unreachable experimentally due to our finite ranges of W and of A. This can be seen by plotting the dependence of the soliton amplitude A on the elliptic parameter m, $A/W = \frac{3}{5}mK^2(m)\delta_{\mathrm{Bo}}\left(\frac{N_\theta W}{\pi R}\right)^2$ from eq. (4), as shown in fig. 6 for different widths W for which elevation solitons are observed. Due to the finite size of the torus, the soliton amplitude is experimentally limited typically to $A/W < 0.2$. As m increases with A, this also limits the reachable values of m, and thus the experimentally reachable solution

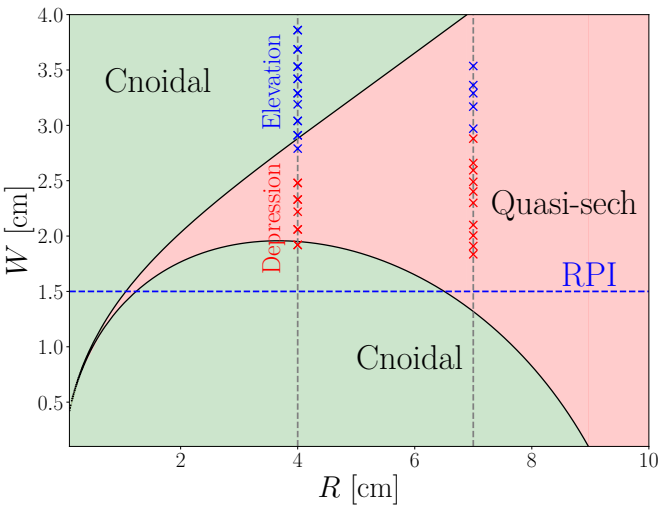

Fig. 7: Phase diagram of the different solutions of the periodic KdV equation. Solid lines: eq. (4) with $A/W = 0.2$, $m = 0.999$ and $N_\theta = 2$. $(\times)$ Torus widths for which depression (red) and elevation (blue) solitons are experimentally observed for the two tested substrates corresponding to a torus radius of $R = 4$ cm or $R = 7$ cm (vertical dashed lines). The torus minimal width is limited by the Plateau–Rayleigh instability (PRI).

types, as corroborated by the results of fig. 5 (*e.g.*, no observation of elevation supersonic soliton for $R = 4$ cm). An equivalent plot to fig. 6 can be obtained for the depression soliton case ($\delta_{\mathrm{Bo}} < 0$, *i.e.*, $\mathrm{Bo} > \mathrm{Bo}_c$) provided that the subsonic and supersonic regions are swapped.

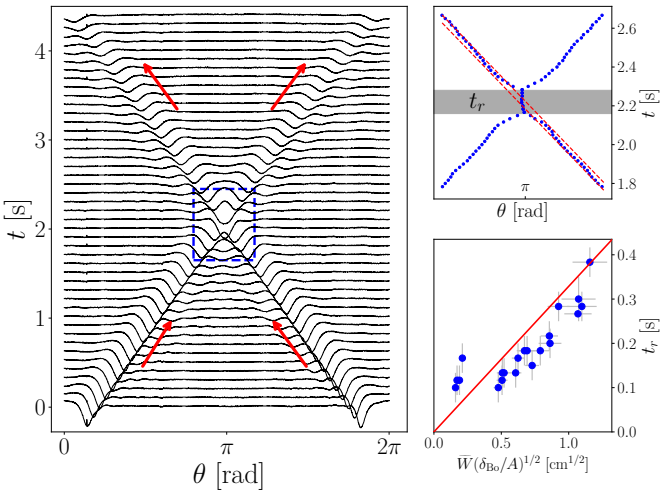

Fig. 8: Angle-time plot of a head-on collision between two depression solitons propagating along a torus. Top: Enlargement (dashed square) showing the soliton minima, phase shift, and residence time t_r. Bottom: t_r vs $\widetilde{W}\sqrt{\delta_{\rm Bo}/A}$ for various A and W. Solid line slope is $0.33\,\mathrm{s/m^{1/2}}$. $R_o = 8.2\,\mathrm{cm}$.

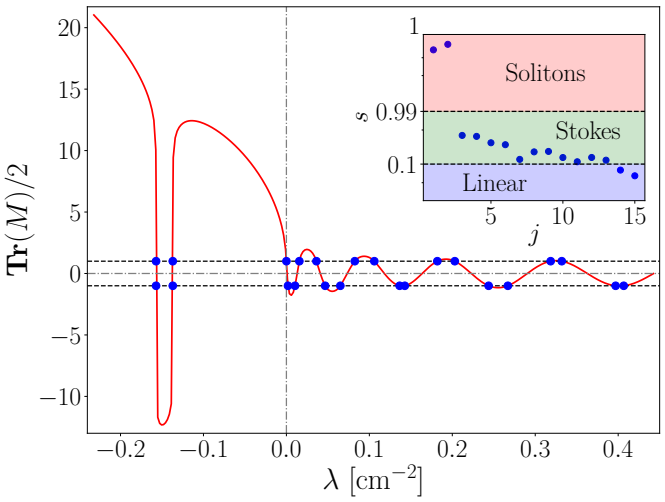

Fig. 9: PIST detection of solitons. $\mathbf{Tr}[M(\lambda)]/2$ (red line) for the signal of fig. 8 at $t_0 = 2.7\,\mathrm{s}$, with the associated nonlinear spectrum (bullets). Two solitons are detected (bullets with $\lambda < 0$). Inset: Soliton index s for different azimuthal wave numbers j revealing two solitons ($s > 0.99$). Lin-Logit scale.

Figure 7 sums up the experimentally observable cases in a phase diagram in the (R,W) parameter space. Inserting the experimental maximal soliton amplitude $A/W = 0.2$, and $m = 0.999$ [separating cnoidal soliton solutions ($m < 0.999$) from quasi-sech ones ($m > 0.999$)], into the periodicity condition of eq. (4) leads to green regions for cnoidal soliton solutions and salmon-pink one for quasi-sech solutions. The experimental data for small tori ($R = 4\,\mathrm{cm}$) fall in both the cnoidal and quasi-sech regions whereas those for a large tori ($R = 7\,\mathrm{cm}$) fall completely in the quasi-sech region, justifying well the velocity observations in fig. 5. Note that, for m far from 1, we still refer to solutions as solitons since they experimentally propagate around the torus as solitary waves and undergo nonlinear interaction, although displaying a nontrivial amplitude dependence velocity (see fig. 5). It is worth noting that, according to eq. (4), the limit of $m = 1$ is unreachable under periodic conditions since it would require an infinite amplitude.

Critical Bond number. – The critical Bond number corresponds to the transition between elevation and depression soliton solutions [10]. It is remarkable that the theoretical value of the critical Bond number $\mathrm{Bo}_c \approx 1/6$ for a torus (see Supp. Mat. [41]) differs from the value 1/3 for the plane geometry case [8]. Indeed, Bo_c strongly depends on the substrate slope α as found numerically [24]. Equating the Bond expression to 1/6 and inserting $\widetilde{W} = R_o - R$, we find the critical outer radius R_o^c of the torus separating elevation and depression solitons as $R_o^{c3} - R_o^{c2}R - \sqrt{6}\ell_{\rm eff}R^2 = 0$, and thus $R_o^c = 8.43\,\mathrm{cm}$ for our parameters. Experimentally, we have a range of $\mathrm{Bo} \in [0.09, 0.5]$ by varying R_o, and we look for the occurrence of the transition from depression ($R_o < R_o^c$) to elevation ($R_o > R_o^c$) solitons by increasing R_o. For small R_o, depression solitons are indeed observed, whereas elevation solitons are detected above a certain radius. We find a critical experimental radius of $R_o^c = 8.4 \pm 0.02\,\mathrm{cm}$ in good agreement with the above predictions. This corresponds to $\mathrm{Bo}_c = 0.17$ close to the theoretical value 1/6. This result is also confirmed when using the other substrate ($R = 4\,\mathrm{cm}$).

Soliton collision. – The nonlinear nature of the solitons is further confirmed by observing the collisions of two depression solitary waves as illustrated in fig. 8. Figure 8 (top right) shows an enlargement of the two solitary wave minima as they collide. The collision evidences a long residence time t_r (of the order of 0.1 s) during collision, and a slight phase shift, a feature of solitons. We experimentally show in fig. (8) (bottom right) that t_r scales as $t_r \sim \widetilde{W}\sqrt{\delta_{\rm Bo}/A}$, matching our prediction (see Supp. Mat. [41]) and extending the pure gravity prediction [45].

Direct scattering. – We have shown above that solitons observed along a liquid torus are well described by eqs. (2)-(4), the solutions of the periodic KdV eq. (1). We now implement a nonlinear spectral analysis, using the periodic inverse scattering transform (PIST), to find the discrete eigenvalue λ of each soliton in our signals [32]. To the best of our knowledge, such a method has not been applied so far to an experimental periodic system with a significant discreteness in Fourier space. We associate with eq. (1) the following eigenvalue problem [32, 37]

$$\psi_{xx} + [\beta\eta(x, t = t_0) + \lambda]\,\psi = 0\,, \qquad (5)$$

subjected to periodic boundary conditions, with period $L = 2\pi R_o$, and $\beta = 5/(12\widetilde{W}^3\chi^2\delta_{\rm Bo})$. The eigenvalues correspond to either bounded solutions, *i.e.*, solitons, for

$\lambda < 0$, and Stokes waves or radiative phonons for $\lambda \geq 0$ [31]. We use a periodic scattering matrix $M(\lambda)$ (called monodromy matrix) to translate the solutions of eq. (5) by one period. The nonlinear spectrum is then given by the condition $\mathbf{Tr}[M(\lambda)]/2 = \pm 1$. The experimental nonlinear spectrum is displayed in fig. 9 (bullets), along with the half-trace of the matrix M (solid line) for the signal in fig. 8 at a time t_0. Two solitons are detected in fig. 9 for which $\mathbf{Tr}[M(\lambda)]/2 = \pm 1$ (four eigenvalues or two band gaps), corresponding to two distinct values $\lambda < 0$. From this nonlinear spectrum, we compute the soliton index s, for each nonlinear mode, as [34]

$$s = \frac{\lambda_{2j+1} - \lambda_{2j}}{\lambda_{2j+1} - \lambda_{2j-1}}, \tag{6}$$

which corresponds to solitons if $s > 0.99$, Stokes waves if $0.5 < s < 0.99$, or linear radiative modes if $s < 0.5$ [46]. We are thus able to count the number of solitons included in a given signal, *e.g.,* the one in fig. 8. Indeed, the inset of fig. 9 confirms the presence of two solitons, as expected. Beyond the validity of PIST to *detect* KdV solitons in a periodic system, PIST could be also be applied to directly *generate* a KdV soliton gas in such a geometry.

Conclusion. – We demonstrated the existence of solitons in a system with periodic and curved boundary conditions. They are observed propagating along a stable torus of fluid (created by a technique we developed) and are fully characterized (profile, velocity, collision, dissipation and nondispersive features). These unexplored solitons are found to be governed by a KdV equation with *periodic boundary conditions* leading to significant differences with infinite straight-line KdV solitons, such as the observation of subsonic elevation solitons, and the prediction of a nonlinear dependence of the soliton velocity on its amplitude. We show that the system periodicity (through the parameter m) selects the soliton velocity type (subsonic or supersonic), whereas the Bond number selects the soliton profile (depression or elevation). A nonlinear spectral analysis of solitons is also implemented (PIST) and is experimentally validated for the first time for a KdV equation with periodic conditions. Our work is not restricted to hydrodynamics, and thus could be applied to other domains involving periodic systems governed by a KdV equation. Quantifying the role of dissipation breaking integrability is also of primary interest [47]. In the future, this new system could address the possible existence of KdV soliton gas [17–21] in periodic systems, and their collision [48], as well as of Kaup-Boussinesq bidirectional solitons [20, 49–51] with corresponding finite-gap spectral methods [52].

* * *

We thank A. Di Palma and Y. Le Goas for technical help on the experimental setup. Part of this work was supported by the French National Research Agency (ANR SOGOOD project No. ANR-21-CE30-0061-04), and by a grant from the Simons Foundation MPS No. 651463.

REFERENCES

[1] Russell J. S., *Proc. R. Soc. Edinburgh*, **11** (1844) 319.
[2] Hao H.-Y. and Maris H. J., *Phys. Rev. B*, **64** (2001) 064302.
[3] Zabusky N. J. and Kruskal M. D., *Phys. Rev. Lett.*, **15** (1965) 240.
[4] Astakhova T. Yu., Menon M. and Vinogradov G. A., *Phys. Rev. B*, **70** (2004) 125409.
[5] Pitaevskii L. and Stringari S., *Bose-Einstein Condensation* (Oxford University Press, Oxford) 2003.
[6] El G. A., Gammal A. and Kamchatnov A. M., *Phys. Rev. Lett.*, **97** (2006) 180405.
[7] Yomosa S., *J. Phys. Soc. Jpn*, **56** (1987) 506.
[8] Korteweg D. J. and de Vries G., *London, Edinburgh, Dublin Philos. Mag. J Sci.*, **39** (1895) 422.
[9] Hammack J. L. and Segur H., *J. Fluid Mech.*, **65** (1974) 289.
[10] Falcon E., Laroche C. and Fauve S., *Phys. Rev. Lett.*, **89** (2002) 204501.
[11] Remoissenet M., *Waves Called Solitons* (Springer-Verlag, Heidelberg, 3rd ed.) 1999.
[12] Dauxois T. and Peyrard M., *Physics of Solitons* (Cambridge University Press, Cambridge) 2006.
[13] Grimshaw R. H. J., *Solitary Waves in Fluids* (WIT-Press, Southampton) 2007.
[14] Novkoski F., Falcon E. and Pham C.-T., *Phys. Rev. Lett.*, **127** (2021) 144504.
[15] Falcon E. and Mordant N., *Annu. Rev. Fluid Mech.*, **54** (2022) 1.
[16] Ricard G. and Falcon E., *EPL (Europhys. Lett.)*, **135** (2021) 64001.
[17] Zakharov V. E., *Sov. Phys. JETP*, **33** (1971) 538.
[18] El G. A. and Kamchatnov A. M., *Phys. Rev. Lett.*, **95** (2005) 204101.
[19] Costa A., Osborne A. R., Resio D. T., Alessio S., Chrivì E., Saggese E., Bellomo K. and Long C. E., *Phys. Rev. Lett.*, **113** (2014) 108501.
[20] Redor I., Barthélemy E., Michallet H., Onorato M. and Mordant N., *Phys. Rev. Lett.*, **122** (2019) 214502.
[21] Suret P., Tikan A., Bonnefoy F., Copie F., Ducrozet G., Gelash A., Prabhudesai G., Michel G., Cazaubiel A., Falcon E., El G. and Randoux S., *Phys. Rev. Lett.*, **125** (2020) 264101.
[22] Bourdin E., Bacri J.-C. and Falcon E., *Phys. Rev. Lett.*, **104** (2010) 094502.
[23] Perrard S., Deike L., Duchêne C. and Pham C.-T., *Phys. Rev. E*, **92** (2015) 011002(R).
[24] Le Doudic G., Perrard S. and Pham C.-T., *J. Fluid Mech.*, **923** (2021) A13.
[25] Shi A., Teng M. H. and Wu T. Y., *J. Fluid Mech.*, **362** (1998) 157.
[26] Elizarova T. G., Istomina M. A. and Shelkovnikov N. K., *Math. Models Comput. Simul.*, **4** (2012) 552.
[27] Perrard S., Couder Y., Fort E. and Limat L., *EPL (Europhys. Lett.)*, **100** (2012) 54006.

[28] Ludu A. and Raghavendra A., *Appl. Numer. Math.*, **141** (2019) 167.
[29] Ait Abderrahmane H., Sedeh P. S., Ng H. D. and Vatistas G. H., *Phys. Rev. E*, **99** (2019) 023110.
[30] Gardner C. S., Greene J. M., Kruskal M. D. and Miura R. M., *Phys. Rev. Lett.*, **19** (1967) 1095.
[31] Ablowitz M. J. and Segur H., *Solitons and the Inverse Scattering Transform* (Society for Industrial and Applied Mathematics, Philadelphia) 1981.
[32] Drazin P. G. and Johnson R. S., *Solitons: An Introduction* (Cambridge University Press, Cambridge) 1989.
[33] Osborne A. R., *Nonlinear Ocean Waves and the Inverse Scattering Transform* (Academic Press, London) 2010.
[34] Christov I., *Math. Comput. Simulat.*, **80** (2009) 192.
[35] Osborne A. R. and Burch T. L., *Science*, **208** (1980) 451.
[36] Redor I., Michallet H., Mordant N. and Barthélemy E., *Phys. Rev. Fluids*, **6** (2021) 124801.
[37] Osborne A. R. and Bergamasco L., *Physica D*, **18** (1986) 26.
[38] Osborne A. R., *Math. Comput. Simulat.*, **37** (1994) 431.
[39] Christov I. C., *Math. Comput. Simulat.*, **82** (2012) 1069.
[40] Gupta R., Vaikuntanathan V. and Sivakumar D., *Colloid. Surface A*, **500** (2016) 45.
[41] See Supplementary Material at ... for (i) movies and (ii) images of solitons propagating along a torus, and additional information on (iii) the form of the KdV equation for a torus, (iv) the residence time during soliton collision, and (v) methods used to obtain the PIST detection.
[42] Novkoski F., Circular border detection in Python, https://github.com/nofko/PYtorus (2020).
[43] Bonn D., Eggers J., Indekeu J., Meunier J. and Rolley E., *Rev. Mod. Phys.*, **81** (2009) 739.
[44] Abramowitz M. and Stegun I. A., *Handbook of mathematical functions with formulas, graphs, and mathematical tables*, Vol. **55** (US Government printing office) 1964.
[45] Power H. and Chwang A. T., *Wave Motion*, **6** (1984) 183.
[46] Osborne A. R., *Phys. Rev. E*, **52** (1995) 1105.
[47] Chekhovskoy I. S., Shtyrina O. V., Fedoruk M. P., Medvedev S. B. and Turitsyn S. K., *Phys. Rev. Lett.*, **122** (2019) 153901.
[48] Carbone F., Dutykh D. and El G. A., *EPL (Europhysics Letters)*, **113** (2016) 30003.
[49] Zhang J. E. and Li Y., *Phys. Rev. E*, **67** (2003) 016306.
[50] Nabelek P. V. and Zakharov V. E., *Physica D*, **409** (2020) 132478.
[51] Congy T., El G. and Roberti G., *Phys. Rev. E*, **103** (2021) 042201.
[52] Smirnov A. O., *Theor. Math. Phys.*, **66** (1986) 19.

Supplementary Material of
Experimental observation of periodic Korteweg-de Vries solitons along a torus of fluid

Filip Novkoski,[1] Chi-Tuong Pham,[2] and Eric Falcon[1]

[1] *Université Paris Cité, CNRS, MSC, UMR 7057, F-75013 Paris, France*
[2] *Université Paris-Saclay, LISN, UMR 9015 CNRS, F-91405 Orsay, France*

In this supplemental material, we present movies (Sec. I) and images (Sec. II) of solitons propagating on a torus of fluid. Details on the form of the Korteweg-de Vries (KdV) equation for a torus (Sec. III) are discussed, which is followed by information on the residence time of a soliton during collision in the capillary case (Sec. IV). Methods used to obtain the nonlinear spectral analysis are described (Sec. V).

I. MOVIES

- soliton_large.mp4 (10 s): Two depression solitons along a torus of width 2.7 cm. $R = 7$ cm substrate.
- soliton_small_depression.mp4 (10 s): Two depression solitons along a torus of width 2.5 cm. $R = 4$ cm substrate.
- soliton_small_elevation.mp4 (12 s): Two elevation solitons along a torus of width 3.4 cm. $R = 4$ cm substrate.

II. IMAGES

- torus_still.png: View of a still torus of liquid on a substrate (groove at $R = 7$ cm).
- torus_soliton.jpg: Two solitons propagating on each border of the torus. Same substrate (groove at $R = 7$ cm).
- torus_small.jpg: View of still torus of liquid on another substrate (groove at $R = 4$ cm).

torus_still.jpg

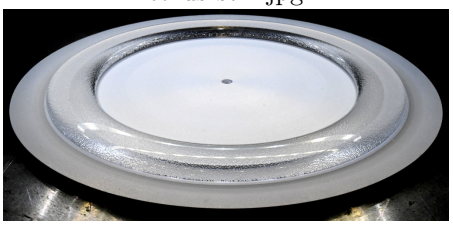

torus_soliton.jpg

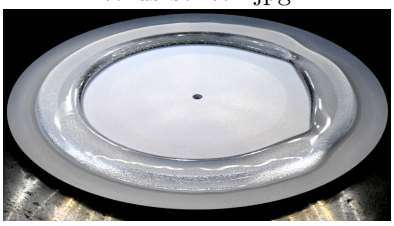

torus_small.jpg

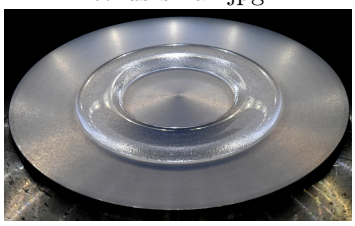

III. KORTEWEG-DE VRIES EQUATION FOR A TORUS

Using the same notation as in the main text, ω the angular frequency and k_θ the azimuthal wave number, the dispersion relation of gravity-capillary waves along a torus of fluid reads

$$\omega^2 = \left(g_{\text{eff}}\frac{k_\theta}{R_o} + \frac{\sigma_{\text{eff}}}{\rho}\frac{k_\theta^3}{R_o^3}\right)\phi\left(\frac{k_\theta}{R_o}\chi^2\widetilde{W}\right). \tag{S1}$$

with $\phi(x)$ a monotonic function that has properties [$\phi(x) \sim x$ for $x \to 0$; $\phi(x) \to 1$ for $x \to \infty$] similar to $\tanh(x)$ [1]. Expanding for $k_\theta \to 0$, using $\phi(x) \approx x - x^3\phi'''(0)/6$, eq. (S1) reads

$$\omega^2 = \Omega_0^2 k_\theta^2\left[1 + \frac{k_\theta^2}{R_o^2}\widetilde{W}^2\chi^2(\text{Bo} - \text{Bo}_c)\right], \tag{S2}$$

with the critical Bond number $\mathrm{Bo}_c = \phi'''(0)/6 \approx 1/6$. After taking the square root of eq. (S2), we find

$$\omega \approx \Omega_0 k_\theta \left[1 + \frac{k_\theta^2}{2R_o^2}\widetilde{W}^2\chi^2(\mathrm{Bo} - \mathrm{Bo}_c)\right]. \tag{S3}$$

By replacing ω and k_θ with $i\partial_t$ and $-i\partial_\theta$ respectively, we recover the linear terms of the KdV eq. (1). We introduce the nonlinear term as in [1], then adapte it for a torus geometry, and normalize it with $\widetilde{W}$. Note that with each k_θ there is an associated factor of χ^2 for the dispersive terms, which leads us to include it within the nonlinear term as well, giving our ansatz KdV eq. (1) in the main text. The numerical factor of $5/4$ comes from the groove shape of the substrate, as numerically and experimentally verified in a straight geometry [1].

IV. RESIDENCE TIME OF COLLISION

For pure gravity waves, *i.e.* $\mathrm{Bo} \ll \mathrm{Bo}_c$, the residence time during a head-on collision between two KdV solitons in a straight geometry is approximately given to the first order by [2]

$$t_r = \ln\left(\frac{\sqrt{3}+1}{\sqrt{3}-1}\right)\frac{2\mu}{k\sqrt{3gh\epsilon}}, \tag{S4}$$

where μ is the dispersion parameter, ϵ is the nonlinearity one, h is the water depth and k is the typical wavenumber. Writing the gravity-capillary KdV eq. (1) in a nondimensional form yields the values of ϵ and μ, and thus

$$t_r = 2\sqrt{\frac{6}{5}}\ln\left(\frac{\sqrt{3}+1}{\sqrt{3}-1}\right)\frac{\widetilde{W}}{\sqrt{g_{\mathrm{eff}}A}}\sqrt{\delta_{\mathrm{Bo}}} \simeq 0.33\left[\mathrm{s/m}^{1/2}\right]\widetilde{W}\sqrt{\frac{\delta_{\mathrm{Bo}}}{A}}, \tag{S5}$$

since the derivation of eq. (S4) is independent of the prefactors in the KdV equation.

V. NUMERICAL METHODS FOR NONLINEAR SPECTRAL ANALYSIS

We largely follow [3, 4] in order to obtain the PIST detection of solitons within our experimental signal. As mentioned before, we are looking for eigenvalues of the associated Schrödinger problem, at fixed time $t = t_0$,

$$\psi_{xx} + [\beta\eta(x, t = t_0) + \lambda]\,\psi = 0, \tag{S6}$$

subjected to periodic boundary conditions, with period $L = 2\pi R_o$, and $\beta = 5/(12\widetilde{W}^3\chi^2\delta_{\mathrm{Bo}})$. Floquet's theorem allows us to write for the fundamental solution matrix Φ as

$$\Phi(x + L; x_0, \lambda) = M(x_0, \lambda)\Phi(x; x_0, \lambda), \tag{S7}$$

where we have introduced the monodromy matrix

$$M(x_0, \lambda) = \begin{pmatrix} a & b \\ b^* & a^* \end{pmatrix}(x_0, \lambda). \tag{S8}$$

It follows that we obtain periodic or antiperiodic solutions when

$$|\,\mathbf{Tr}(M)| = 2. \tag{S9}$$

In practice we consider a signal $\eta(x)$ consisting of N points on an interval discretized by Δx. Since we do not have direct access to the monodromy matrix, we are led to look at the following closely related scattering matrix

$$S = \prod_{i=N-1}^{0} T \quad \text{where} \quad T = \begin{pmatrix} \cos(k\Delta x) & \sin(k\Delta x)/k \\ -k\sin(k\Delta x) & \cos(k\Delta x) \end{pmatrix}(x, \lambda), \tag{S10}$$

where $k = \sqrt{\beta\eta(x) + \lambda}$. The monodromy matrix M and the above scattering matrix are related through

$$\mathbf{Tr}(M) = \mathbf{Tr}(S), \tag{S11}$$

$$M_{21} = S_{12}. \tag{S12}$$

For a given signal $\eta(x)$, with $N = 3801$, we calculate the matrix S and its trace for each value of λ in an interval $[\lambda_{\min}, \lambda_{\max}]$, where $\lambda_{\min} = -\beta[\max(\eta) - \langle\eta\rangle_x]$ and $\lambda_{\max} = \lambda_{\min} + 2|\lambda_{\min}|$, in order to obtain Fig. 6 of the main paper.

To obtain the soliton spectrum of Fig. 6, we look for zeros of $|\,\mathbf{Tr}(M)|/2 - 1$. This is done by first finding the maxima and minima for a set of $|\,\mathbf{Tr}(M)|/2$ calculated on N points in the given interval. We use the pairs of λ of those extrema as bounds for the bisection method, through which we then find the zeros to a tolerance of 10^{-12}. These methods should remain valid, despite the bidirectionality of the system, as long as solitons are locally KdV [5], namely far enough from interacting with each other.

REFERENCES

[1] Le Doudic G., Perrard S. and Pham C.-T., *J. Fluid Mech.*, **923** (2021) A13.
[2] Power H. and Chwang A. T., *Wave Motion*, **6** (1984) 183.
[3] Osborne A. R. and Burch T. L., *Science*, **208** (1980) 451.
[4] Osborne A. R. and Bergamasco L., *Physica D*, **18** (1986) 26.
[5] Zhang J. E. and Li Y., *Phys. Rev. E*, **67** (2003) 016306.